



Original Article

Estimating Facet Joint Apposition with Specimen-Specific Computer Models of Subaxial Cervical Spine Kinematics

RYAN D. QUARRINGTON ¹, DARCY W. THOMPSON-BAGSHAW,^{1,2}
and CLAIRE F. JONES^{1,2}

¹Adelaide Spinal Research Group, Centre for Orthopaedic & Trauma Research, Adelaide Medical School, The University of Adelaide, Level 7, Adelaide Health and Medical Sciences Building, North Terrace, Adelaide, SA 5000, Australia; and ²School of Mechanical Engineering, The University of Adelaide, Adelaide, Australia

(Received 9 July 2021; accepted 4 November 2021; published online 17 November 2021)

Associate Editor Stefan M. Duma oversaw the review of this article.

Abstract—Computational models of experimental data can provide a noninvasive method to estimate spinal facet joint biomechanics. Existing models typically consider each vertebra as one rigid-body and assume uniform facet cartilage thickness. However, facet deflection occurs during motion, and cervical facet cartilage is nonuniform. Multi rigid-body computational models were used to investigate the effect of specimen-specific cartilage profiles on facet contact area estimates. Twelve C6/C7 segments underwent non-destructive intervertebral motions. Kinematics and facet deflections were measured. Three-dimensional models of the vertebra and cartilage thickness estimates were obtained from pre-test CT data. Motion-capture data was applied to two model types (2RB: C6, C7 vertebrae each one rigid body; 3RB: left and right C6 posterior elements, and C7 vertebrae, each one rigid body) and maximum facet mesh penetration was compared. Constant thickness cartilage (CTC) and spatially-varying thickness cartilage (SVTC) profiles were applied to the facet surfaces of the 3RB model. Cartilage apposition area (CAA) was compared. Linear mixed-effects models were used for all quantitative comparisons. The 3RB model significantly reduced penetrating mesh elements by accounting for facet deflections ($p = 0.001$). The CTC profile resulted in incongruent facet articulation, whereas realistic congruence was observed for the SVTC profile. The SVTC profile demonstrated significantly larger CAA than the CTC model ($p < 0.001$).

Keywords—Cartilage, Apposition, Neck.

ABBREVIATIONS

CTC	Constant thickness cartilage
SVTC	Spatially-varying thickness cartilage
CAA	Cartilage apposition area

INTRODUCTION

The interaction between articulating subaxial cervical facets prevents excessive intervertebral anterior shear, axial rotation, and lateral bending motions,⁵ protecting the spinal cord and contributing to intervertebral kinematics. The facets are often fractured during neck injury,⁹ suggesting high load transmission through these joints due to inter-facet interaction. It is likely that the magnitude and region of this facet joint apposition dictates neck kinematics and the risk of facet dislocation and/or fracture during cervical trauma. Furthermore, some evidence suggests that changes to facet mechanics (including apposition) due to degeneration^{10,32} and surgical intervention,^{20,30} lead to facet joint disease. However, there is currently limited information regarding subaxial cervical facet joint apposition changes during physiologic and traumatic intervertebral motions.

The few studies that have measured inter-facet joint mechanics in *ex vivo* cadaveric cervical spines have used invasive techniques, inserting piezoresistive pressure sensors^{23,34,37} and probes^{15,16} into the joint space. The compromise of the joint capsule that is typically

Address correspondence to Ryan D. Quarrington, Adelaide Spinal Research Group, Centre for Orthopaedic & Trauma Research, Adelaide Medical School, The University of Adelaide, Level 7, Adelaide Health and Medical Sciences Building, North Terrace, Adelaide, SA 5000, Australia. Electronic mail: ryan.quarrington@adelaide.edu.au

required to insert these sensors, combined with the sensors' interaction with the articulating surfaces, likely alters joint kinematics⁴² and leads to overestimated joint apposition.^{2,18} Such methods are also typically limited to measuring facet joint apposition in the region of the sensor and do not detect interaction in other areas of the joint.

Computational reconstructions of experimental data and finite element (FE) analyses are non-invasive methods to quantify spine mechanics parameters that are difficult to measure directly, such as facet joint apposition area. FE models have been used to estimate the effect of surgical interventions^{36,38,41} and anatomical asymmetry²⁹ on facet joint mechanics, but the osseous geometry of FE models is typically reconstructed from medical images of a *single healthy individual*, which is unlikely to represent the variation within the general population. While they are able to investigate the effect of an expanded matrix of input and boundary conditions, FE models are also computationally intensive, and require accurate definition of tissue material properties and extensive validation against experimental data. In contrast, rigid-body computational reconstructions of experimental kinematic data have been used to estimate cervical spine mechanics that are technically challenging to measure directly, including canal occlusion¹³ and facet joint kinematics.^{14,22} Similar techniques are yet to be applied to measure facet joint apposition in the cervical spine.

Computational reconstructions of flexion-extension motions applied to *lumbar* spines (L1-sacrum) have been used to calculate facet joint apposition at each spinal level throughout physiological range of motion. Specimen-specific rigid-body models of each vertebra were developed from computed tomography (CT) scans, and optical motion capture data was individually applied to each level to recreate the experimental kinematics.⁶ Each vertebral body and its posterior elements were considered as a single rigid-body; however, over 14° of sagittal bending relative to the vertebral body has been observed during replicated *physiological* intervertebral flexion of the lumbar facets.¹¹ This suggests that this rigid-body assumption may be violated even within physiological loading bounds. In the cervical spine, bending of the posterior elements relative to the vertebral body has been observed during simulated physiological^{25,26} and traumatic^{25,27} intervertebral motions, but these deflections are not typically considered in computational reconstructions of spinal motion.^{6,12,14,22,33} Deflection of the posterior elements may occur *in vivo* due to inter-facet contact forces and loading by the capsular ligament, therefore are likely important for biofidelic simulations of intervertebral cervical motion; however, the extent to which posterior element deflection affects

computational estimates of facet and cartilage apposition area has not previously been investigated.

In most computer models of the spine, the facet cartilage is assumed to have constant thickness across the osseous surface,^{6,29,35} but articular cartilage thickness is non-uniform in the cervical spine.³⁹ Spatially-varying cartilage profiles have been incorporated into recent advanced FE human neck models.⁷ These profiles provided more accurate predictions of facet joint apposition when compared to the constant thickness model,³⁷ but this investigation was limited to a single cervical spine specimen. The effect of anatomically accurate, joint-specific cartilage profiles on cervical spine facet joint apposition area estimations from computational reconstructions of experimental data has not been investigated.

The aims of this project were to use specimen-specific C6/C7 computational reconstructions of experimental kinematic data to: (1) determine the effect of incorporating C6 inferior facet deflections on the fidelity of the reconstruction; and, (2) compare facet joint apposition area estimates obtained with a constant thickness versus variable thickness articular cartilage profile.

METHODS

Experimental Data

Subaxial cervical motion segments (C5-T1 or C6/C7) were dissected from twelve fresh-frozen human cadavers (mean donor age 70 ± 13 years, range 46–88; nine male) and non-osteoligamentous tissue was removed. The C6/C7 spinal level was of interest in this study as it is most commonly dislocated (with or without an accompanying facet fracture) during neck trauma.²⁸ Six radiopaque, 2 mm diameter aluminium spheres (fiducial markers; Mingliang Steel Ball Factory, Guangzhou, China) were rigidly attached to each of the C6 and C7 vertebrae; three in the vertebral bodies and three in the spinous processes (12 total) using a custom bead insertion device and cyanoacrylate adhesive (Loctite 401, Henkel, Düsseldorf, Germany). Care was taken to ensure that the locations of the fiducials inserted into each vertebra were non-collinear, and were attached to both the left and right sides of the specimen. Specimens underwent high-resolution computed tomography (CT) scanning (SOMATOM Force, Siemens, Erlangen, Germany; $0.23 \times 0.23 \times 0.4$ mm voxel size) to screen for C6/C7 joint fusions or osteophytes that may limit intervertebral motion, spinal injury or disease, and to generate three-dimensional (3D) specimen-specific osseous models of the C6 and C7 vertebrae.

The distal ends of each specimen were embedded in molds with polymethylmethacrylate (Vertex Dental, Utrecht, Netherlands) while maintaining the C6/C7 intervertebral joints and discoligamentous tissues. Custom, light-weight, motion capture marker carriers were attached bilaterally to the inferolateral corners of the C6 inferior facets using cyanoacrylate adhesive (Loctite 401, Henkel, Düsseldorf, Germany), and were rigidly fixed to the C6 and C7 vertebral bodies with K-wires. Each specimen then underwent non-destructive constrained shear and bending motions, superimposed with three axial loading conditions, as previously described.²⁶ Only kinematic data from the “neutral” axial condition (50 N axial compression force to replicate head-weight)^{4,8} tests were used to address the aims of the current study as this loading condition was most similar to that applied in previous work, allowing for valid comparison of outputs.³⁷ Briefly, a six-axis materials testing machine (8802, Instron, High Wycombe, UK) was used to apply three repetitions of anterior shear (limit: 1 mm; rate: 0.1 mm/s), flexion (10°; 1°/s), right axial rotation (4°; 1°/s) and left lateral bending (5°; 1°/s). The displacement/rotation limits were based on *in-vivo* ranges of motion^{19,24,31,40} and displacement rates were optimized relative to motion-capture sampling rate. A two-second position “hold” was applied at the peak of each rotation/displacement, over which test outcomes were averaged. Axial force was monitored using a six-axis load cell (MC3A-6-1000 ± 4.4 kN, AMTI, Massachusetts, USA).

Prior to testing, the location of each fiducial marker was digitized relative to their respective vertebral body marker carrier using a four-marker wand (Optotrak Certus, Northern Digital Inc., ON, Canada) with a custom 1 mm diameter spherical probe tip. Anatomical landmarks on the left and right C6 inferior facets were digitized relative to their respective marker carriers. Digitization was performed while the specimen was in an “unloaded” position (< 10 N axial compression, all other loads/moments ~ 0 N/Nm). Motion capture data were acquired at 200 Hz (Optotrak Certus, Northern Digital Inc., Ontario, Canada; system bias < 0.09°, precision = 0.006°). The six-axis materials testing machine actuator positions were collected at 600 Hz using a data acquisition system (PXIe-1073, BNC-2120 & PXIe-4331 (×2), National Instruments, USA).

Experimental data were processed using custom MATLAB code (R2020a, Mathworks, MA, USA). All data were filtered using a second-order, two-way Butterworth low-pass filter; a cut-off frequency of 100 Hz was used for actuator positions, and 30 Hz was used for motion capture data.

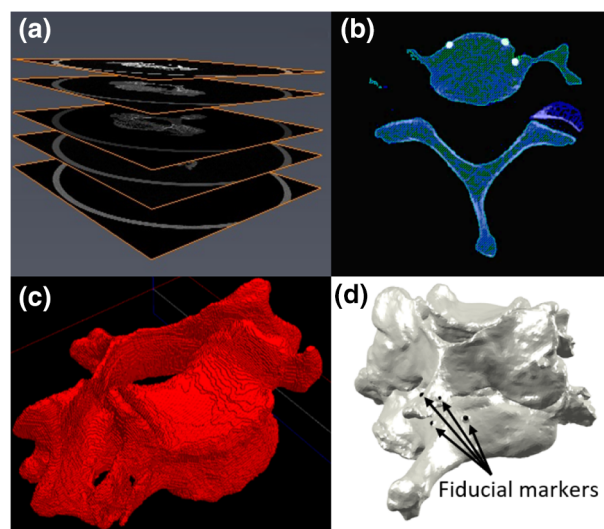


FIGURE 1. Generating the specimen-specific computer models: (a) computed tomography scan data of C6 and C7 vertebra were imported into 3D analysis software; (b) bone and fiducial marker geometries were segmented from the CT data; (c) surface mesh data of the vertebra and markers were generated and exported; and, (d) the models were imported into MATLAB.

Generating Specimen-Specific Computer Models

Three-dimensional osseous models of C6 and C7 were generated from the high-resolution CT scans (Fig. 1a) of each specimen using 3D image analysis software (Amira 6.4.0, Thermo Fisher Scientific, Massachusetts, USA). The C6 and C7 vertebrae, their corresponding fiducial markers, and the bilateral C6 inferior and C7 superior facet osseous articular surfaces, were segmented semi-automatically based on pixel intensity and anatomical landmarks (Fig. 1b). Mesh resolution was varied on a subset of models in order to establish model convergence, and the optimum element parameters were determined; triangular surface mesh data (vertex coordinates and connectivity list; mean element surface area and edge lengths = 0.025 mm² and 0.22 mm, respectively) were exported (Fig. 1c). The mesh data were then imported into MATLAB and transformed from the CT coordinate system to the motion capture (experimental) coordinate system (Fig. 1d) by co-registering the locations of three or more fiducial markers (with the specimen in the “unloaded” position) using Procrustes analysis without scaling (MATLAB function “Procrustes”).

Applying Motion Capture Data to Model

Motion-capture data was applied to the C6/C7 rigid-body models to recreate the intervertebral motions applied in the experiments. To address Aim 1, two methods of recreating the vertebral kinematics were applied: the Two Rigid-Body (2RB); and, the Three

Rigid-Body (3RB) methods. The 2RB method assumed that the C6 and C7 vertebrae (vertebral body + posterior elements) each acted as a rigid-body. The 3RB method accounted for deflections of the left and right C6 inferior facets, relative to the vertebral body,^{25,26} by modelling C6 as three separate rigid-bodies: the vertebral body, and the two (bilateral) inferior facets (Fig. 2). Due to the anatomy of the C6/C7 facet joints (and surrounding structures), attaching marker carriers to the C7 facets was not possible; this necessitated that the C7 vertebrae was modelled as a single rigid-body.

Procrustes analysis was used to determine the transformation matrix between successive frames of motion capture data, for each rigid-body (Fig. 3). For both methods, the three *vertebral body fiducial marker locations* were used to determine the C6 and C7 vertebral body transformations, and the C6 inferior facet *landmarks* were used to transform the facet surface meshes for the 3RB method; these transformations were applied to the corresponding models in the experimental coordinate system. This process was applied to all experimental data to generate computational reconstructions of the kinematics of the C6 and C7 vertebral bodies (2RB & 3RB), and the C6 inferior facets (including specimen-specific cartilage; 3RB only) for each of the experimental motions.

Calculating Facet Penetration

To evaluate the fidelity of the 2RB and 3RB computational reconstructions, the amount of penetration of the bony facets within each joint (which cannot occur *in-vivo*) was evaluated. Throughout each test, the maximum number of penetrating mesh elements of each facet joint was determined for each modelling method, for statistical comparison. The most biofidelic rigid-body modelling method was then used to investigate the effect of two different cartilage profiles on facet apposition area calculations.

Applying Cartilage Profile to Facet Articular Surfaces

As cartilage was not observed on the CT images, the articular cartilage profiles on each facet surface were estimated. Two previously reported cartilage models were applied to the articulating C6 inferior and C7 superior osseous facet surfaces of each model to evaluate their effect on apposition area while the specimen was in the neutral posture.

For the Constant Thickness Cartilage (CTC) model, uniform thickness cartilage layers were applied across the osseous bone surfaces of the C6 inferior and C7 superior facets (0.5 and 0.6 mm, respectively). These values were informed by cartilage thickness measure-

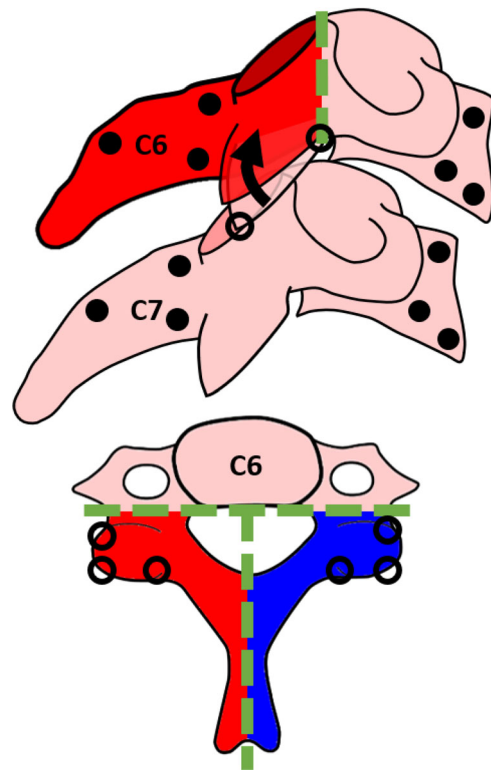


FIGURE 2. Lateral (top) and inferior (bottom) view illustrations of the two rigid-body (2RB; pink) and three rigid-body (3RB; pink, red, and blue) models. Bending of the right C6 inferior facet during the 3RB simulations is illustrated by the black arrow in the lateral view. The locations of the fiducial markers (closed dots) and anatomical landmarks (open dots), which were used to determine the transformations between subsequent experimental frames, are indicated.

ments obtained from histology of ~ 100 lower cervical spine facets, from seven human cadavers.³⁹

Spatially-varying Thickness Cartilage (SVTC) profiles were generated by applying a three-dimensional thickness mapping function (Eq. (1)), derived from histological analysis of lower cervical spine cartilage,³⁹ to the C6 inferior and C7 superior facet osseous surfaces.

$$t = t_{\max} \cdot \cos^k \left(\frac{\pi}{2} r_{\text{ratio}} \right) \quad (1)$$

In Eq. (1), the cosine term causes the cartilage profile to transition from zero thickness around the entire perimeter of the articular surface, to the maximum thickness (t_{\max}) at the facet center. The shape parameter (k) is an empirically determined constant which dictates the rate of change of cartilage thickness. It is specific to the spinal level and varies slightly for the inferior and superior facets of the joint; $k = 0.47$ and 0.49 for the C6 inferior and C7 superior facets, respectively.³⁹ r_{ratio} is the ratio of the radial distance

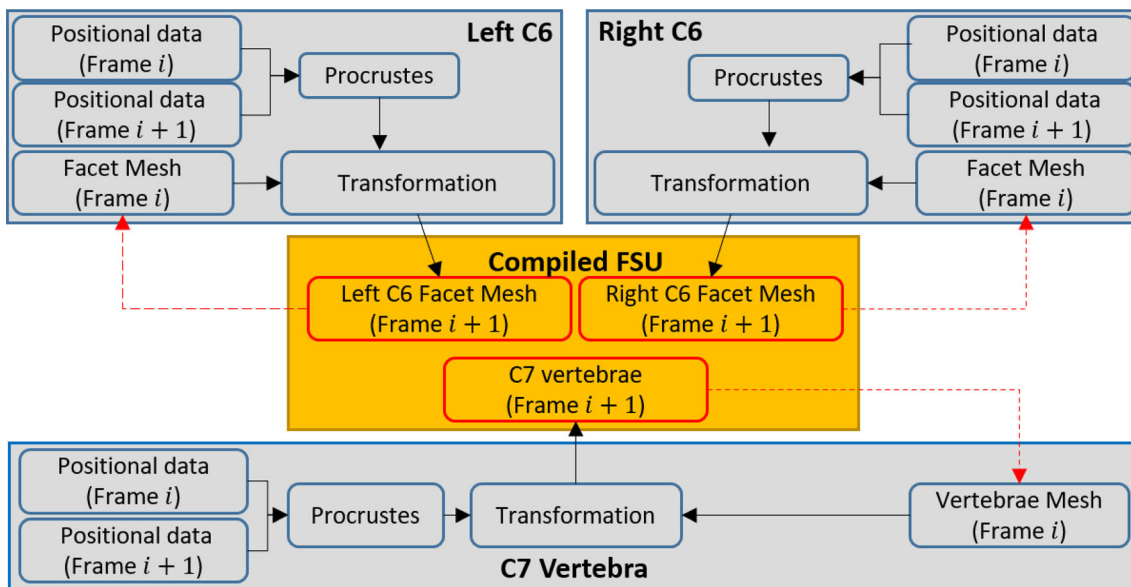


FIGURE 3. The three rigid-body (3RB) transformation workflow. Linear transformations between subsequent frames were calculated from the motion capture data and applied to each rigid-body (left C6 facet, right C6 facet, and C7 vertebra). The C6 vertebral body was not included as only the C6 inferior facet positions and motions were required to calculate facet articulation.

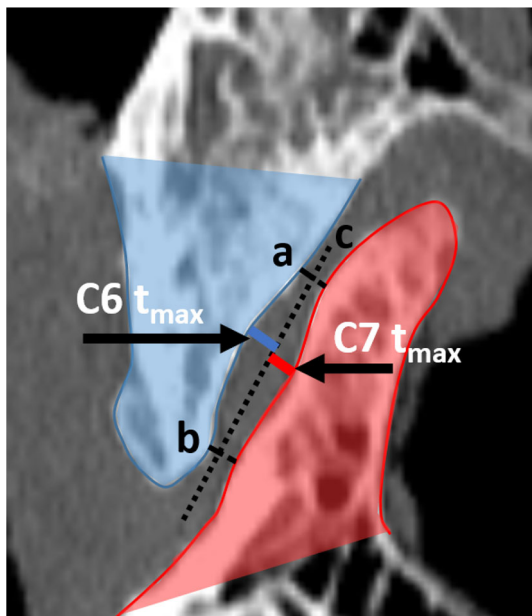


FIGURE 4. For each facet, maximum cartilage thickness (t_{\max}) was estimated from mid-sagittal CT slices of the facet joint as follows: (1) lines were drawn between the anterior (a) and posterior (b) edges of the articulating surfaces of the C6 and C7 facets; (2) the midpoints of each of these lines were connected (c) to define the “midline” of the facet joint space; (3) t_{\max} C6 and C7 were defined as the largest distance between the corresponding facet and the midline, normal to the facet surface.

from a point on the surface, to the co-linear radial distance from the perimeter. The maximum thickness value (t_{\max}) applied was specimen and facet-specific,

and was estimated from high-resolution mid-sagittal CT slices of each facet joint (Fig. 4) using image processing software (RadiAnt DICOM Viewer, Medixant, Poznan, Poland). Measurements were recorded by two observers on two separate occasions, and inter- and intra-observer reliability analyses were performed.³

For each cartilage model, a custom MATLAB function was used to extrude the profile in the direction normal to the osseous articular surface of each facet, for each vertebra (Fig. 5). The CTC and SVTC models of each specimen were saved separately for investigating the effect of cartilage profile on facet apposition area.

Calculating Facet Apposition Area

Custom MATLAB code was developed to measure facet apposition at each joint by summing intersecting and penetrating cartilage mesh elements. Elements from the upper cartilage mesh that intersected or penetrated the opposing cartilage mesh were deemed to be articulating. The corresponding apposition area was calculated by projecting the articulating elements onto a plane that was fitted to the regions of apposition (Fig. 6). Graphical representations of the articulating and non-articulating regions of each joint were produced to qualitatively assess the fidelity of each cartilage profile. The total area of the projected elements was evaluated for each facet joint to calculate the transient facet joint cartilage apposition area (CAA). The mean CAA for the first 100 frames of each test (while the specimen was statically loaded in the neutral

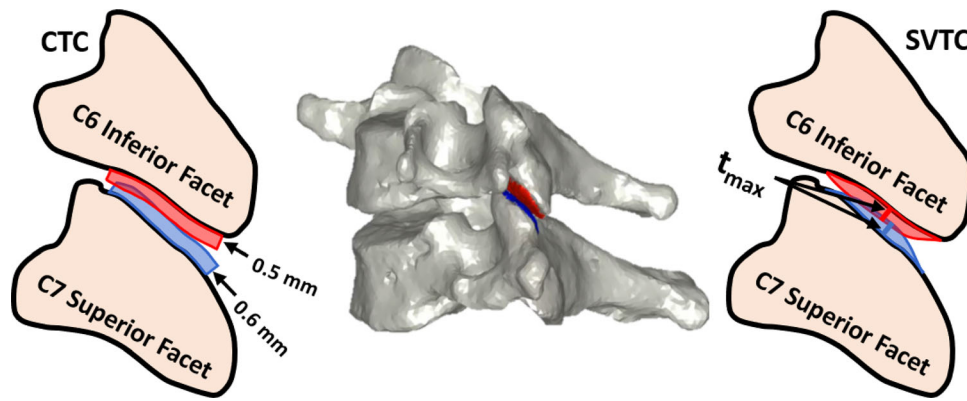


FIGURE 5. Mid-sagittal cross-section illustrations of the C6/C7 facet joint with the constant thickness cartilage (CTC; left) and spatially varying thickness cartilage profiles (SVTC; right). These cartilage profiles were extruded from the osseous articular surface of each facet, for each specimen-specific model (center).

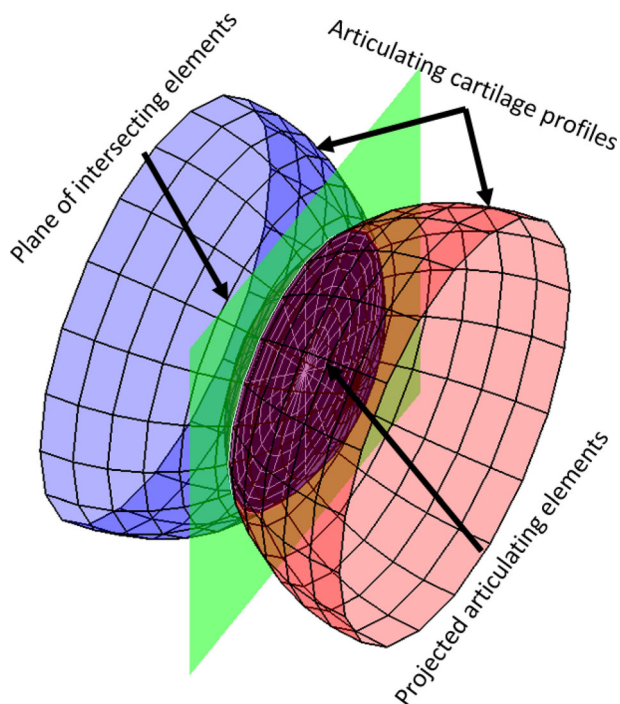


FIGURE 6. Exaggerated illustration of the method used to determine cartilage apposition area (CAA). A plane (green rectangle) was fitted to elements from the opposing cartilage meshes that were “articulating” (intersecting or overlapping). The articulating elements were then projected onto the plane, and the area of this projection was the CAA.

position; $CAA_{neutral}$) was compared for the cartilage profile methods.

Statistics

Statistical analyses were performed using SPSS v26 (IBM, IL, USA). Linear mixed-effects models (LMMs) evaluated the difference in facet mesh penetration between the 2RB and 3RB models, and the change in $CAA_{neutral}$ between the facets with CTC versus SVTC

Facet Mesh Penetration for Each Rigid Body Method

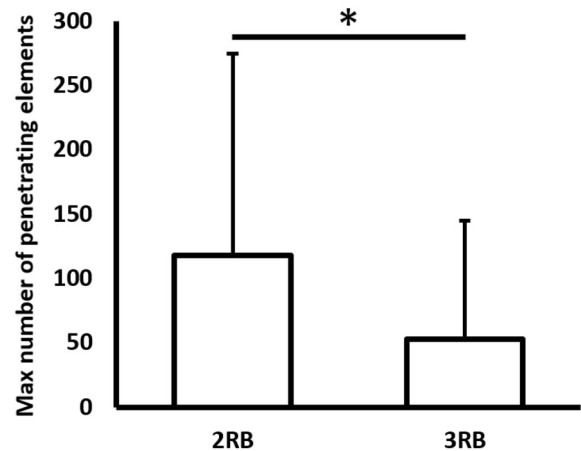


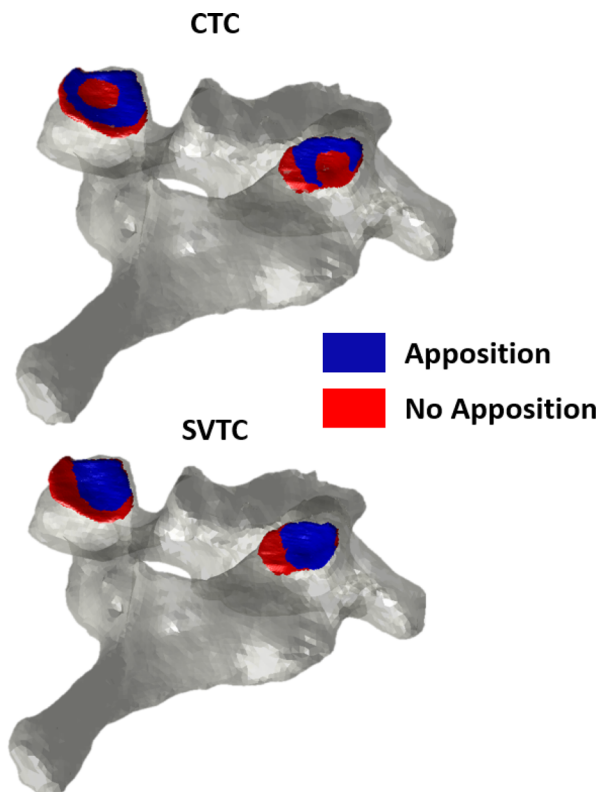
FIGURE 7. Mean (\pm SEM) of maximum number of penetrating facet mesh elements for each facet joint ($n = 23$), throughout an entire test, for the two rigid-body (2RB) and three rigid-body (3RB) computer models. Significant difference indicated ($\alpha = 0.05$).

profiles. For both LMMs, the effect of rigid-body and cartilage modelling method, respectively, was adjusted for facet side (left versus right), and a random effect of facet side nested within cadaver identifier was included.

Interobserver agreement and intraobserver repeatability of t_{max} measurements were evaluated using intraclass correlation coefficients (ICCs).³ Absolute agreement and consistency of ICC measures were obtained. The following thresholds were used to interpret ICC values: > 0.8 , almost perfect agreement; $0.61-0.8$, substantial agreement; $0.41-0.6$, moderate agreement; $0.21-0.4$, fair agreement; and $0-0.2$, slight agreement.¹⁷

TABLE 1. Maximum cartilage thickness measurements for each facet, for each specimen.

Specimen ID	Maximum cartilage thickness (mm)			
	C6 L	C7 L	C6 R	C7 R
H002	1.05	0.50	1.30	0.81
H003	1.93	1.35	1.82	1.26
H004	–	–	1.11	1.09
H009	0.63	0.55	0.55	0.43
H010	1.24	0.98	1.47	1.42
H013	1.42	1.14	1.41	1.55
H014	1.22	0.94	1.19	0.83
H020	1.93	1.26	1.24	1.37
H033	0.90	0.82	0.89	1.03
H036	1.27	0.85	1.16	1.15
H041	0.74	0.99	0.47	0.68
H043	0.90	0.85	1.24	0.55
Mean \pm SD	1.20 \pm 0.43	0.93 \pm 0.26	1.15 \pm 0.38	1.01 \pm 0.36

**FIGURE 8.** Cartilage apposition areas for the constant thickness cartilage (CTC; top) and spatially varying thickness cartilage (SVTC; bottom) profiles for Specimen H020, displayed on the superior facets of C7.

RESULTS

Of the twelve computer models generated, the left facet joint of one specimen (H004) was excluded because of pathological joint morphology; the C7 osseous surface was flat rather than convex which reduced the maximum joint space substantially (< 1 mm). The

osseous surfaces of all other facets were comprised of 6138 ± 1796 mesh elements.

The 3RB modelling method resulted in a significantly lower maximum number of penetrating facet bone mesh elements compared to the 2RB method (Fig. 7; Table S1; $p = 0.001$). This penetration occurred in 75% of tests for the 2RB method, compared to 58% for the 3RB method (Table S2). When mesh penetration did occur (regardless of rigid-body method), the maximum penetration was most often during anterior shear (43%) or axial rotation (35%) motions, and never occurred during intervertebral flexion.

Intra-class correlation analysis demonstrated at least good agreement for inter-rater and intra-rater measurements of maximum cartilage thickness from CT (Table S3). Maximum cartilage thickness measurements ranged between 0.47 and 1.93 mm for the C6 facets, and 0.43 and 1.55 mm for the C7 facets (Table 1).

In general, the CTC profile resulted in apposition around the perimeter of the articular surface of the facet, with an absence of articulating cartilage in the center. In contrast, the SVTC profile created an even distribution of apposition (Fig. 8). As a result, the SVTC profile demonstrated significantly larger $CAA_{neutral}$ compared to the CTC method (Fig. 9; $p < 0.001$); when adjusting for specimen type and ID, this difference was 6.6 mm^2 (30.6%; 28.2 ± 2.5 vs. $21.6 \pm 2.5 \text{ mm}^2$; Table S4).

DISCUSSION

Computer reconstructions of experimental kinematic data offer a non-invasive method of investigating the biomechanics of anatomical structures that cannot be directly visualized or instrumented. This is partic-

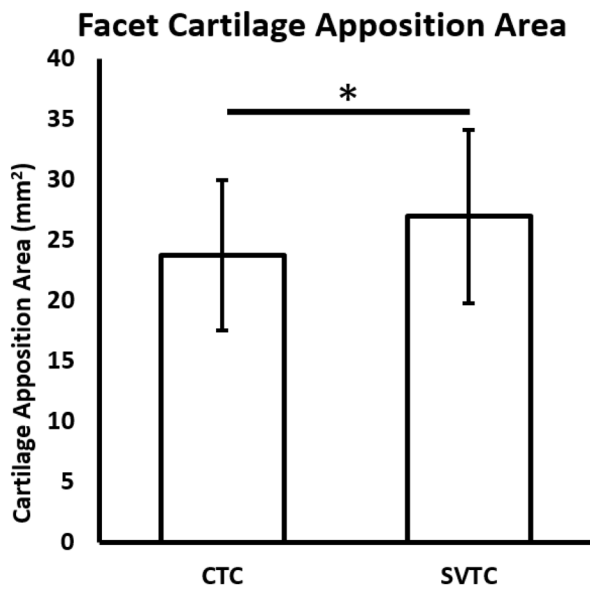


FIGURE 9. Mean (\pm SEM) of facet cartilage apposition area for the Constant Thickness Cartilage (CTC) and Spatially Varying Thickness Cartilage (SVTC) profiles ($n = 23$). Significant difference indicated ($\alpha = 0.05$).

ularly important when exploring synovial joint mechanics, as alterations to the capsule or the articulating surfaces may change joint kinematics.⁴² Existing kinematic models of the human cervical spine have limited utility for investigating facet joint mechanics, as they consider each vertebra to be a single rigid-body,^{6,12,14,22,33} while FE models often apply a cartilage layer of constant thickness across the osseous articular surface.^{6,29,35} In the current study, incorporating specimen-specific facet deflections and spatially-varying cartilage profiles significantly reduced non-physiologic bone penetration, and produced more uniform estimates of facet joint apposition area, respectively. It is likely that these factors would affect predictions of other facet biomechanical parameters (e.g., contact force, pressure), so future computer reconstructions of spinal motion data should consider posterior element deflections and include specimen-specific cartilage profiles.

Inter-facet contact forces occur during physiologic and traumatic motions of the cervical spine, causing bending of the posterior elements relative to the vertebral body.^{25,26} If this bending is not replicated during non-contact computational reconstructions, and each vertebra is modelled as a single rigid-body, the facet meshes will overlap, leading to erroneous joint apposition area calculations. In the current study, the fidelity of the 2RB and 3RB models was evaluated by measuring the amount of bony penetration of the facets. Sagittal-plane facet deflections of over 1.5° were applied to the 3RB models,²⁶ resulting in a significantly

reduced overlap of the opposing facet meshes compared to the 2RB models (Fig. 7). Overlap still occurred for 58% of 3RB tests (Table S1), and this always occurred at peak motion, likely due to the inability of the method to account for bending of the *C7 superior* facets; however, measuring these facet deflections is extremely challenging in practice.

Simplified, non-anatomical cartilage profiles applied to computational models of the cervical spine produce inaccurate facet joint apposition area and contact pressure estimates³⁷, leading to substantially different predictions in facet joint kinematics and disc strain.⁷ For synovial joints such as the spinal facets, congruency of opposing articular cartilage surfaces distributes joint contact forces to reduce local stresses.³⁷ In the subaxial cervical spine, the osseous surfaces of each facet curve away from the joint space (both concave, relative to the joint space) in the sagittal plane (Fig. 4).³⁹ Therefore, the bony joint surfaces are non-congruent, creating an approximately elliptical “void” within the joint space that is thickest at the middle. As a result, when the CTC profile was applied to anatomically accurate bone models the cartilage surfaces did not articulate in the central region of the joint; in contrast, the SVTC profile provided a more consistent congruence of cartilage apposition across all regions (Fig. 8), as is expected for healthy joints, and this resulted in significantly larger $CAA_{neutral}$ compared to that for the CTC profile (Fig. 9).

The SVTC apposition area estimates in the current study were comparable to those measured by piezoresistive pressure sensors placed within the C4/C5 and C5/C6 facet joints (mean = 29.9 ± 23.3 vs. 27.0 ± 7.13 mm² in the current study) of C3–C7 human cadaver cervical spine segments under 40 N of axial compression, while in the neutral posture³⁷; the authors are not aware of similar apposition area data for the C6/C7 facet joints, but osseous surface area and cartilage thickness profiles do not vary substantially throughout the subaxial cervical spine.^{21,39} Although not explicitly stated, it is assumed that these apposition measurements required a portion of the facet capsule to be resected to insert each sensor, which likely altered joint kinematics during intervertebral motions⁴²; however, the capsule should not influence facet mechanics when compression is applied to spinal segments in the “neutral” posture, so comparison against these measured values would be most suited to validation.²⁶

Despite good agreement with published facet joint articulation area measurements, the lack of specimen-specific validation is a limitation of the current study. Ideally, direct measurements of CAA would have been obtained post-test, from pressure sensors (or similar) inserted into the C6/C7 facet joint, to provide a

“ground truth” for comparisons. This was not possible in the current study, as it was designed to complement a series of experimental studies in which the specimens were eventually subjected to destructive testing.²⁷ As such, these models are best suited for use in repeated measures analyses to evaluate the effect of (for example) variations in specimen anatomy, surgical intervention, and changes in external loading, on facet joint apposition area.

The cartilage models applied in the current study did not incorporate hyperelastic material properties, so any cartilage deformation that may have occurred during facet articulation was not represented. Compressive loading of unconstrained articular cartilage causes an initial lateral expansion of the tissue,¹ which may have resulted in a slight increase in CCA at the periphery of the facet joints; however, the CAA_{neutral} values produced were similar to those measured experimentally and estimated by Womack *et al.*'s validated model (approximately 20 mm²),³⁷ suggesting that the proposed reconstruction pipeline accurately estimates facet joint apposition from experimental kinematic data.

Three-dimensional facet cartilage geometry could not be segmented for the specimens in this study because the soft tissues of the joint were not clearly visible on the CT images, and subsequent destructive experiments precluded direct measurement of the cartilage following testing. Instead, spatially-varying thickness mapping functions were applied to the C6 inferior and C7 superior osseous articular facet surfaces (Eq. 1). These level-specific profiles were derived from histological measurements of ~100 subaxial cervical facets,³⁹ and contact area estimates from computational models incorporating these profiles have previously been validated against measurements from pressure maps inserted into 24 human cadaver subaxial cervical facet joints.³⁷ In the current study, specimen-specific t_{\max} values were estimated for each facet from measurements of the joint space on parasagittal CT images. These maximum cartilage thickness estimates were comparable to measurements obtained from serial histological sectioning of facets from seven human cadaver cervical spines ($n = 14$ per level; C6 inferior = 1.17 ± 0.39 vs. 0.94 ± 0.23 mm; C7 superior = 0.97 ± 0.30 vs. 1.14 ± 0.17 mm).³⁹

A small co-registration “offset error” was introduced by the distance between the tip of the digitizing wand (used to determine the fiducial marker coordinates in the experimental reference frame) and the fiducial marker centroid (diameter = 2 mm; calculated from the CT-extracted point cloud of each marker). The maximum possible positional difference (offset error) between a pair of fiducial markers would occur if they were digitized on geometrically opposite sides,

and could amount to at least the diameter of a marker (2 mm). However, this potential digitization/transformation error was minimized by using a highly accurate Optotrak system (positional accuracy 0.01 mm), small diameter fiducial markers to minimize the offset distance, and iterative Procrustes analysis for co-registration. In the current study, the Procrustes function was used to determine the transformation matrix that transformed the CT-derived fiducial marker locations to best-fit the fiducial marker coordinates digitised in the experimental space (with the specimen in the “unloaded” posture). Using this method, a linear translation aligned the center position (i.e., mean location) of the CT coordinates with that of the digitised points, and the best-fit rotation matrix minimized the *total* offset error (cumulative for all marker pairs); scaling was not permitted so that the model's anatomical geometry was maintained. For each vertebra, this Procrustes analysis was iteratively performed for every combination of ≥ 3 markers (of the 6 per vertebra) to determine the combination that produced the transformation that best fit the motion capture coordinates. On average, the co-registration *total* offset error amongst all specimens was 0.65 ± 0.17 mm (less than half the diameter of a fiducial marker), which indicated excellent accuracy of the reconstruction pipeline.

In this study, posterior element deflections of C6 were accounted for by considering the vertebral body and posterior elements as separate rigid bodies. The rigid-body assumptions are violated if a fracture occurs through part of the body, so facet joint apposition cannot be accurately estimated following a facet fracture. This limits the utility of this method for injury biomechanics research, but facet mechanics during traumatic injury are typically not of interest beyond the point of bony failure.

The results of the current study demonstrate the importance of accounting for posterior element deflections, and specimen-specific articular cartilage profiles, in computational models of the subaxial cervical spine. Including these factors significantly improved the fidelity of the computer simulations and the estimates of cartilage apposition area, which could alter predictions of cervical spine biomechanics. The non-invasive method of estimating facet joint apposition area used in the current study, which also accounted for facet deflections, could be applied to longer spinal segments and used to estimate changes in apposition area during experimental investigations of cervical spine trauma, or due to surgical implants and interventions. This information would provide valuable insight into the biomechanics underlying traumatic spinal injuries such as facet dislocation, assess the ability of spinal implants (such as intervertebral disc replacements) to recreate non-pathologic facet

joint mechanics, and investigate adjacent level effects following surgical intervention.

SUPPLEMENTARY INFORMATION

The online version contains supplementary material available at <https://doi.org/10.1007/s10439-021-02888-8>.

ACKNOWLEDGMENTS

The authors thank Fraser Darcy for his contributions towards developing the 3D meshes of each cervical spine motion segment and acknowledge the facilities, and scientific and technical assistance, of the National Imaging Facility, a National Collaborative Research Infrastructure Strategy (NCRIS) capability, at the South Australian Health and Medical Research Institute Clinical Research and Imaging Centre.

CONFLICT OF INTEREST

The authors declare that no benefits in any form have been or will be received from a commercial party related directly or indirectly to the subject of this manuscript.

REFERENCES

- ¹Armstrong, C. G., W. M. Lai, and V. C. Mow. An analysis of the unconfined compression of articular cartilage. *J. Biomech. Eng.* 106(2):165–173, 1984. <https://doi.org/10.1115/1.3138475>.
- ²Bachus, K. N., A. L. DeMarco, K. T. Judd, D. S. Horwitz, and D. S. Brodke. Measuring contact area, force, and pressure for bioengineering applications: using Fuji Film and TekScan systems. *Med. Eng. Phys.* 28(5):483–488, 2006. <https://doi.org/10.1016/j.medengphy.2005.07.022>.
- ³Bartlett, J. W., and C. Frost. Reliability, repeatability and reproducibility: analysis of measurement errors in continuous variables. *Ultrasound Obstet. Gynecol.* 31(4):466–475, 2008. <https://doi.org/10.1002/uog.5256>.
- ⁴Bell, K. M., Y. Yan, R. E. Debski, G. A. Sowa, J. D. Kang, and S. Tashman. Influence of varying compressive loading methods on physiologic motion patterns in the cervical spine. *J. Biomech.* 49(2):167–172, 2016. <https://doi.org/10.1016/j.jbiomech.2015.11.045>.
- ⁵Bogduk, N., and S. Mercer. Biomechanics of the cervical spine. I: normal kinematics. *Clin. Biomech. (Bristol, Avon)*. 15(9):633–648, 2000.
- ⁶Cook, D. J., and B. C. Cheng. Development of a model based method for investigating facet articulation. *J. Biomech. Eng.* 132(6):064504, 2010. <https://doi.org/10.1115/1.4001078>.
- ⁷Corrales, M. A., and D. S. Cronin. Importance of the cervical capsular joint cartilage geometry on head and facet joint kinematics assessed in a finite element neck model. *J. Biomech.* 123:110528, 2021. <https://doi.org/10.1016/j.jbiomech.2021.110528>.
- ⁸DiAngelo, D. J., and K. T. Foley. An improved biomechanical testing protocol for evaluating spinal arthroplasty and motion preservation devices in a multilevel human cadaveric cervical model. *Neurosurg. Focus.* 17(3):E4, 2004.
- ⁹Dvorak, M. F., C. G. Fisher, B. Aarabi, et al. Clinical outcomes of 90 isolated unilateral facet fractures, subluxations, and dislocations treated surgically and nonoperatively. Comparative Study Research Support, Non-U.S. Gov't. *Spine.* 32(26):3007–3013, 2007. <https://doi.org/10.1097/BRS.0b013e31815cd439>.
- ¹⁰Edwards, C. C., II., K. D. Riew, P. A. Anderson, A. S. Hilibrand, and A. F. Vaccaro. Cervical myelopathy. Current diagnostic and treatment strategies. *Spine J.* 3(1):68–81, 2003.
- ¹¹Green, T. P., J. C. Allvey, and M. A. Adams. Spondylolysis. Bending of the inferior articular processes of lumbar vertebrae during simulated spinal movements. Research Support, Non-U.S. Gov't. *Spine.* 19(23):2683–2691, 1994.
- ¹²Havey, R. M., J. Goodsitt, S. Khayatadeh, et al. Three-dimensional computed tomography-based specimen-specific kinematic model for ex vivo assessment of lumbar neuroforaminal space. *Spine.* 40(14):E814–E822, 2015. <https://doi.org/10.1097/brs.0000000000000959>.
- ¹³Ivancic, P. C., A. M. Pearson, Y. Tominaga, A. K. Simpson, J. J. Yue, and M. M. Panjabi. Mechanism of cervical spinal cord injury during bilateral facet dislocation. *Spine (Phila Pa 1976)*. 32(22):2467–2473, 2007. <https://doi.org/10.1097/BRS.0b013e3181573b67>.
- ¹⁴Ivancic, P. C., A. M. Pearson, Y. Tominaga, A. K. Simpson, J. J. Yue, and M. M. Panjabi. Biomechanics of cervical facet dislocation. *Traffic Injury Prev.* 9(6):606–611, 2008. <https://doi.org/10.1080/15389580802344804>.
- ¹⁵Jaumard, N. V., J. A. Bauman, C. L. Weisshaar, B. B. Guarino, W. C. Welch, and B. A. Winkelstein. Contact pressure in the facet joint during sagittal bending of the cadaveric cervical spine. *J. Biomech. Eng.* 133(7):071004, 2011. <https://doi.org/10.1115/1.4004409>.
- ¹⁶Jaumard, N. V., J. A. Bauman, W. C. Welch, and B. A. Winkelstein. Pressure measurement in the cervical spinal facet joint: considerations for maintaining joint anatomy and an intact capsule. *Spine (Phila Pa 1976)*. 36(15):1197–1203, 2011. <https://doi.org/10.1097/BRS.0b013e3181ee7de2>.
- ¹⁷Landis, J. R., and G. G. Koch. The measurement of observer agreement for categorical data. *Biometrics.* 33(1):159–174, 1977.
- ¹⁸Liau, J. J., C. C. Hu, C. K. Cheng, C. H. Huang, and W. H. Lo. The influence of inserting a Fuji pressure sensitive film between the tibiofemoral joint of knee prosthesis on actual contact characteristics. *Clin. Biomech. (Bristol, Avon)*. 16(2):160–166, 2001.
- ¹⁹Lin, C. C., T. W. Lu, T. M. Wang, C. Y. Hsu, S. J. Hsu, and T. F. Shih. In vivo three-dimensional intervertebral kinematics of the subaxial cervical spine during seated axial rotation and lateral bending via a fluoroscopy-to-CT registration approach. *J. Biomech.* 47(13):3310–3317, 2014. <https://doi.org/10.1016/j.jbiomech.2014.08.014>.
- ²⁰Murtagh, R. D., R. M. Quencer, D. S. Cohen, J. J. Yue, and E. L. Sklar. Normal and abnormal imaging findings in lumbar total disk replacement: devices and complications.

- RadioGraphics*. 29(1):105–118, 2009. <https://doi.org/10.1148/rg.291075740>.
- ²¹Panjabi, M. M., T. Oxland, K. Takata, V. Goel, J. Duranceau, and M. Krag. Articular facets of the human spine. Quantitative three-dimensional anatomy. *Spine (Phila Pa 1976)*. 18(10):1298–1310, 1993. <https://doi.org/10.1097/00007632-199308000-00009>.
- ²²Panjabi, M. M., A. K. Simpson, P. C. Ivancic, A. M. Pearson, Y. Tominaga, and J. J. Yue. Cervical facet joint kinematics during bilateral facet dislocation. *Eur. Spine J.* 16(10):1680–1688, 2007. <https://doi.org/10.1007/s00586-007-0410-2>.
- ²³Patel, V. V., Z. R. Wuthrich, K. C. McGilvray, et al. Cervical facet force analysis after disc replacement versus fusion. *Clin. Biomech. (Bristol, Avon)*. 44:52–58, 2017. <https://doi.org/10.1016/j.clinbiomech.2017.03.007>.
- ²⁴Penning, L., and J. T. Wilmink. Rotation of the cervical spine. A CT study in normal subjects. *Spine*. 12(8):732–738, 1987.
- ²⁵Quarrington, R. D., J. J. Costi, B. J. C. Freeman, and C. F. Jones. Quantitative evaluation of facet deflection, stiffness, strain and failure load during simulated cervical spine trauma. *J. Biomech.* 72:116–124, 2018. <https://doi.org/10.1016/j.jbiomech.2018.02.036>.
- ²⁶Quarrington, R. D., J. J. Costi, B. J. C. Freeman, and C. F. Jones. The effect of axial compression and distraction on cervical facet mechanics during anterior shear, flexion, axial rotation, and lateral bending motions. *J. Biomech.* 83:205–213, 2019. <https://doi.org/10.1016/j.jbiomech.2018.11.047>.
- ²⁷Quarrington, R. D., J. J. Costi, B. J. C. Freeman, and C. F. Jones. Investigating the effect of axial compression and distraction on cervical facet mechanics during supraphysiologic anterior shear. *J. Biomech. Eng.* 2021. <https://doi.org/10.1115/1.4050172>.
- ²⁸Quarrington, R. D., C. F. Jones, P. Tcherveniakov, et al. Traumatic subaxial cervical facet subluxation and dislocation: epidemiology, radiographic analyses, and risk factors for spinal cord injury. *Spine J.* 18(3):387–398, 2018. <https://doi.org/10.1016/j.spinee.2017.07.175>.
- ²⁹Rong, X., B. Wang, C. Ding, et al. The biomechanical impact of facet tropism on the intervertebral disc and facet joints in the cervical spine. *Spine J.* 17(12):1926–1931, 2017. <https://doi.org/10.1016/j.spinee.2017.07.009>.
- ³⁰Ryu, K.-S., C.-K. Park, S.-C. Jun, and H.-Y. Huh. Radiological changes of the operated and adjacent segments following cervical arthroplasty after a minimum 24-month follow-up: comparison between the Bryan and Prodisc-C devices. *J. Neurosurg. Spine*. 13(3):299, 2010. <https://doi.org/10.3171/2010.3.spine09445>.
- ³¹Salem, W., C. Lenders, J. Mathieu, N. Hermanus, and P. Klein. In vivo three-dimensional kinematics of the cervical spine during maximal axial rotation. *Man Ther.* 18(4):339–344, 2013. <https://doi.org/10.1016/j.math.2012.12.002>.
- ³²Serhan, H. A., G. Varnavas, A. P. Dooris, A. Patwardhan, and M. Tzermiadianos. Biomechanics of the posterior lumbar articulating elements. *Neurosurg. Focus*. 22(1):1, 2007. <https://doi.org/10.3171/foc.2007.22.1.1>.
- ³³Smith, Z. A., S. Khayatzaadeh, J. Bakhsheshian, et al. Dimensions of the cervical neural foramen in conditions of spinal deformity: an ex vivo biomechanical investigation using specimen-specific CT imaging. *Eur. Spine J.* 25(7):2155–2165, 2016. <https://doi.org/10.1007/s00586-016-4409-4>.
- ³⁴Stieber, J. R., M. Quirno, M. Kang, A. Valdevit, and T. J. Errico. The facet joint loading profile of a cervical intervertebral disc replacement incorporating a novel saddle-shaped articulation. *J. Spinal Disord. Tech.* 24(7):432–436, 2011. <https://doi.org/10.1097/BSD.0b013e3182027297>.
- ³⁵Teo, E. C., and H. W. Ng. Evaluation of the role of ligaments, facets and disc nucleus in lower cervical spine under compression and sagittal moments using finite element method. *Med. Eng. Phys.* 23(3):155–164, 2001.
- ³⁶Wang, Z., H. Zhao, J. M. Liu, L. W. Tan, P. Liu, and J. H. Zhao. Resection or degeneration of uncovertebral joints altered the segmental kinematics and load-sharing pattern of subaxial cervical spine: a biomechanical investigation using a C2–T1 finite element model. *J. Biomech.* 49(13):2854–2862, 2016. <https://doi.org/10.1016/j.jbiomech.2016.06.027>.
- ³⁷Womack, W., U. M. Ayturk, and C. M. Puttlitz. Cartilage thickness distribution affects computational model predictions of cervical spine facet contact parameters. *J. Biomech. Eng.* 133(1):011009, 2011. <https://doi.org/10.1115/1.4002855>.
- ³⁸Womack, W., P. D. Leahy, V. V. Patel, and C. M. Puttlitz. Finite element modeling of kinematic and load transmission alterations due to cervical intervertebral disc replacement. *Spine (Phila Pa 1976)*. 36(17):E1126–E1133, 2011. <https://doi.org/10.1097/BRS.0b013e31820e3dd1>.
- ³⁹Womack, W., D. Woldtvedt, and C. M. Puttlitz. Lower cervical spine facet cartilage thickness mapping. *Osteoarthritis Cartilage*. 16(9):1018–1023, 2008. <https://doi.org/10.1016/j.joca.2008.01.007>.
- ⁴⁰Wu, S. K., L. C. Kuo, H. C. Lan, S. W. Tsai, C. L. Chen, and F. C. Su. The quantitative measurements of the intervertebral angulation and translation during cervical flexion and extension. *Eur. Spine J.* 16(9):1435–1444, 2007. <https://doi.org/10.1007/s00586-007-0372-4>.
- ⁴¹Yuchi, C. X., G. Sun, C. Chen, et al. Comparison of the biomechanical changes after percutaneous full-endoscopic anterior cervical discectomy versus posterior cervical foraminotomy at C5–C6: a finite element-based study. *World Neurosurg.* 2019. <https://doi.org/10.1016/j.wneu.2019.05.025>.
- ⁴²Zdeblick, T. A., J. J. Abitbol, D. N. Kunz, R. P. McCabe, and S. Garfin. Cervical stability after sequential capsule resection. *Spine (Phila Pa 1976)*. 18(14):2005–2008, 1993. <https://doi.org/10.1097/00007632-199310001-00013>.

Publisher's Note Springer Nature remains neutral with regard to jurisdictional claims in published maps and institutional affiliations.